nature photonics

Article

https://doi.org/10.1038/s41566-023-01321-x

Laser pulse compression by a density gradient plasma for exawatt to zettawatt lasers

Received: 24 November 2022

Accepted: 29 September 2023

Published online: 13 November 2023

Check for updates

Min Sup Hur[1] ✉, Bernhard Ersfeld[2], Hyojeong Lee[3], Hyunsuk Kim[1], Kyungmin Roh[3], Yunkyu Lee[1], Hyung Seon Song[1], Manoj Kumar[1], Samuel Yoffe[2], Dino A. Jaroszynski[2] ✉ & Hyyong Suk[3] ✉

We propose a new method of compressing laser pulses to ultrahigh powers based on spatially varying dispersion of an inhomogeneous plasma. Here, compression is achieved when a long, negatively frequency-chirped laser pulse reflects off the density ramp of an over-dense plasma slab. As the density increases longitudinally, high-frequency photons at the leading part of the laser pulse penetrate more deeply into the plasma region than lower-frequency photons, resulting in pulse compression in a similar way to that by a chirped mirror. Proof-of-principle simulations performed using particle-in-cell simulation codes predict compression of a 2.35 ps laser pulse to 10.3 fs—a ratio of 225. As plasma is robust and resistant to damage at high intensities—unlike solid-state gratings commonly used in chirped-pulse amplification—the method could be used as a compressor to reach exawatt or zettawatt peak powers.

The invention of the chirped-pulse amplification (CPA) technique[1] has made the development of ultrashort pulse, multipetawatt laser systems possible. Petawatt pulses are useful for compact plasma-based multigigaelectronvolt electron accelerators[2] and hundreds-of-megaelectronvolt ion accelerators[3], which are usually only available at large-scale accelerator facilities. By extending laser powers to the exawatt scale (1 EW = 10^{18} W), pulses from these systems would provide tools that are capable of experimentally investigating various modern theoretical physics problems, such as pair production[4], photon–photon scattering[5], radiation reaction[6], and in-laboratory reproduction of the early universe[7]. Zettawatt (1 ZW = 10^{21} W) laser pulses would exceed the Schwinger limit[8] and address the paradox of information loss in black holes[9].

Yet zettawatt lasers are unlikely to be soon realized using current CPA techniques because the manufacture of large-size compression gratings is almost at its technological limit. Even for petawatt-level pulse compression, metre-scale gratings are required to ensure that the pulse intensity does not exceed their surface damage thresholds. By simple extrapolation, diameters of gratings for exawatt or zettawatt lasers would be hundreds of metres. This poses enormous challenges that are in turn encouraging a search for fundamentally different approaches to compression. As material damage presents the major obstacle on the path towards post-exawatt powers, a plasma-based compression scheme is very appealing, because plasma is an already broken-down state of matter and is fundamentally resistant to damage by the high electric fields of intense laser pulses. The maximum energy density sustainable by plasma is several orders of magnitude higher (~10^{17} W cm^{-2}) than that of solid-state media (~10^{13} W cm^{-2})[10,11]. This means that a huge grating could potentially be replaced by a plasma mirror that is several orders of magnitude smaller, if a method can be found to make the plasma dispersive. Raman and Compton amplification are promising plasma-based methods for pulse compression[12–19]. In these schemes, a long-duration pump laser pulse is backward-scattered and compressed by an electron plasma wave; the plasma wave is self-generated under the action of the ponderomotive force of the beat wave associated with the pump and counter-propagating seed

[1]Department of Physics, Ulsan National Institute of Science and Technology, Ulsan, Republic of Korea. [2]Department of Physics, Scottish Universities Physics Alliance and University of Strathclyde, Glasgow, UK. [3]Department of Physics and Photon Science, Gwangju Institute of Science and Technology, Gwangju, Republic of Korea. ✉e-mail: mshur@unist.ac.kr; d.a.jaroszynski@strath.ac.uk; hysuk@gist.ac.kr

pulse (forming the compressed pulse). Compression of a 25-ps-long, 4 TW (>100 J) pulse into 25 fs, 2 PW (~50 J) (with an efficiency of 35%) has been observed in particle-in-cell (PIC) simulations[17]. Experimentally, compression of joule-level pulses (~50 J) was first demonstrated with 10% efficiency[19]. A slower, but more robust amplification mechanism by Brillouin scattering has also been studied[20]. Generation of plasma gratings by beating two counter-propagating laser pulses as a compressor has been suggested[21–25]. Small-factor compression using plasma gratings has been demonstrated in PIC simulations[23,24], but more substantial breakthroughs are yet to come.

Here we introduce a fundamentally different approach. Our method is much simpler and, most importantly, much more efficient than other proposed plasma-based schemes. We predict that a long, chirped pulse can be compressed several hundred times to achieve intensities of $I \approx 10^{17}$ W cm^{-2}, with almost no energy loss, using a millimetre-size plasma grating, which is orders-of-magnitude smaller than those of conventional CPA systems. By further optimization, it is expected that even zettawatt powers may be obtainable from a compact system.

Basic idea

The plasma-based schemes of laser pulse compression described in the introduction use plasma that has a layered density profile to scatter a pump pulse; however, plasma is an intrinsically dispersive medium, even without a periodic structure. Here we propose a new and more direct way of exploiting the dispersive property of plasma for pulse compression. The dispersion relation of an electromagnetic wave of frequency ω and wave number k in plasma is given by $\omega^2 = \omega_p^2 + c^2k^2$, where the plasma frequency $\omega_p \propto \sqrt{n_0}$, and n_0 is the plasma density; the group velocity of photons therefore depends on frequency. Most importantly, a photon is reflected at the point where its frequency is equal to ω_p; photons with higher frequency are reflected at locations of higher density. Therefore, when a negatively frequency-chirped laser pulse is incident on a plasma slab with an increasing density gradient, higher-frequency photons have longer round-trip paths than lower-frequency ones, resulting in compression of the laser pulse (Fig. 1). Examples of one-dimensional (1D) PIC simulations show that a 2.35 ps (FWHM), frequency-chirped ($\Delta\omega/\omega = 0.13$) Gaussian laser pulse with a peak intensity of $I_0 = 8.5 \times 10^{14}$ W cm^{-2} increases to $I = 9.8 \times 10^{16}$ W cm^{-2} (a factor of 115-times larger) in a 2.5-mm-long plasma-grating that has a quadratically increasing density profile. In Supplementary Figs. 1–3 we demonstrate up to 50-fold compression in two- and quasi-three-dimensional simulations. Past studies[10,11] have shown that the damage threshold of conventional gratings in CPA is about 10^{13} W cm^{-2}. By contrast, the intensity of the compressed laser pulse in our simulation is about four orders of magnitude higher than that of conventional CPA compressors. This implies that plasma with a density gradient, and a diameter of only 10 cm, can be used to reach 7.7 EW laser power, which is unprecedented. In other simulations that we have performed, we have obtained a 225-fold increase in the intensity, which corresponds to 2.3 EW for the same assumed diameter. Our idea shares the common principle of group-delay dispersion with dispersive mirrors[26], but the major difference of using plasma instead of a dielectric opens up new possibilities for exawatt-and-above high-power lasers in the future.

Simulation results

Figure 2 presents a 1D PIC simulation result showing a 225-fold gain in intensity—from $I_0 = 1.37 \times 10^{14}$ W cm^{-2} to $I = 3.05 \times 10^{16}$ W cm^{-2}—due to pulse compression. The incident pulse (red in Fig. 2a) with a duration of 2.35 ps full-width at half-maximum (FWHM) is compressed to 10.3 fs FWHM (blue). The incident laser pulse is longitudinally Gaussian, $\sim \exp\left[-t^2/\tau_\sigma{}^2\right]$, with a cut-off at $1.5\tau_\sigma$. The pulse duration is set to $\tau_\sigma = 2$ ps (2.35 ps FWHM). The angular frequency is negatively chirped starting from $\omega_h = 2.73 \times 10^{15}$ rad s^{-1} ($\lambda_h = 690$ nm), sweeping linearly to $\omega_l = 1.86 \times 10^{15}$ rad s^{-1} ($\lambda_l = 1{,}010$ nm). The corresponding relative bandwidth $\Delta\omega_{FHWM}/\omega_c = 0.13$ indicates a Fourier-limited pulse of 9.8 fs, which would be the minimum pulse duration possible by compression. Here the subscripts h, l and c are used to indicate the highest, lowest and central frequencies or densities, respectively. A cold ($T_e = 0$) plasma slab is loaded with a quadratically increasing density profile given by the function $n(x) = n_h(x - x_0)^2/L^2$, where we set $L = 1.81$ mm, $x_0 = 0.3$ mm (plasma–vacuum boundary) and $n_h = 2.35 \times 10^{21}$ cm^{-3} (n_h is the critical density for ω_h). The density ramp is extended to $1.5n_h$ to minimize leakage of pulse energy beyond the critical point through the skin depth layer. Simulation particles are loaded by the cumulative distribution technique[27] to minimize artificial noise in the density profile. Note that, for a quadratic density profile, the round-trip time of photons is a linear function of frequency (that is, $\int_0^{l_c} v_g^{-1} dx \propto \omega$, where l_c is the critical point and v_g is the photon's group velocity), which is compatible with compression of linearly chirped pulses.

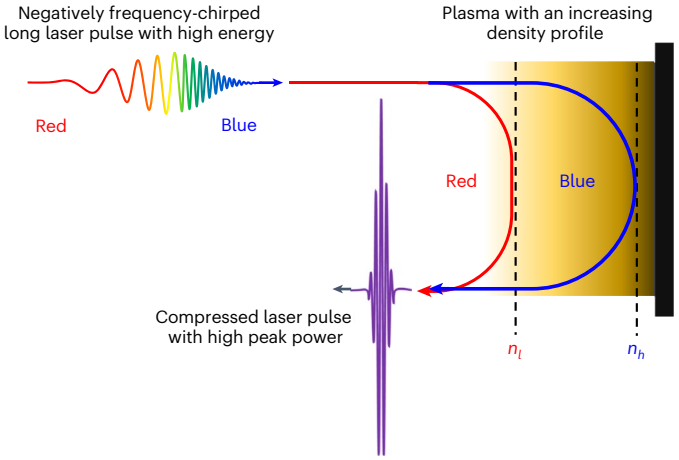

Fig. 1 | A concept of pulse compression in a plasma. The laser pulse compressor based on a density gradient plasma, in which a long-duration, high-energy, negatively frequency-chirped laser pulse reflects from an over-dense plasma slab with an increasing density ramp. High-frequency components at the front of the pulse and low frequency components at the rear part of the pulse reflect at different positions, leading to compression of the laser pulse.

In the simulation, a virtual probe is placed at $x = 0.1$ mm (vacuum side) to detect the electric field as a function of time (Fig. 2b), and evaluate the frequency spectra of both the incident and reflected pulses (Fig. 2d). The probed data are split into three sections: the incident pulse (red in Fig. 2b), the compressed pulse (blue) and the pre-backscattered portion by Raman backscatter (RBS) in the middle (orange). The compressed pulse (Fig. 2c) comprises 99.2% of the incident energy. The original spectrum of the incident pulse is well preserved in the compressed pulse (Fig. 2d). Only a small portion of the incident energy is lost via RBS (Fig. 2b,d).

Raman backscatter is more deleterious in warm plasma compared with cold plasma, as the thermal noise can trigger RBS much earlier. Figure 3 shows simulation results from a thermal plasma at a temperature of 10 eV, in which we have kept all other parameters the same as in Fig. 2. A substantial portion of the rear part of the pulse is depleted by RBS (Fig. 3a–c). With RBS growth, the longitudinal electric field E_x (red in Fig. 3a–c) grows in a similar way to the incident pulse amplitude and persists throughout the compression process (Fig. 3d,e). Note that RBS is triggered at the quarter-critical density, that is, when $n = n_{1/4} = 0.25n_c$ (n_c is the critical density for the central frequency ω_c), at which the growth rate of RBS is also maximum. The peak amplitude (~3.7×10^{11} V m^{-1}) after the compression is slightly reduced compared with the cold case (Fig. 3k). Of the incident pulse energy, 75% is compressed, whereas 16% is scattered by RBS. The remaining 9% is

https://doi.org/10.1038/s41566-023-01321-x

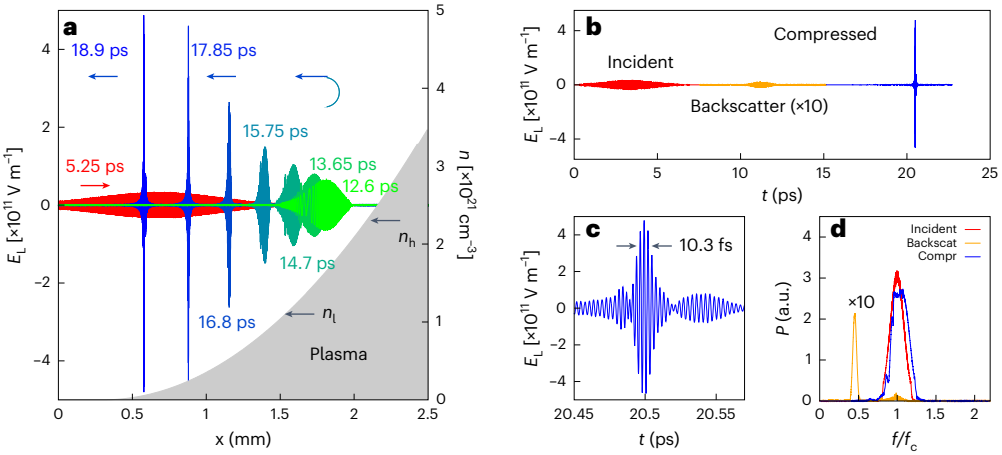

Fig. 2 | Pulse compression in a gradient plasma from a 1D PIC simulation. **a**, Incident pulse (red) and stroboscopic view of the reflected pulse (green to blue). On the plasma density profile (grey shade), n_h and n_l are the critical densities for ω_h (the highest frequency at the front tip of the pulse) and ω_l (the lowest frequency at the rear tip of the pulse), respectively. **b**, Electric field passing through a virtual probe located at $x = 0.1$ mm as a function of time. The data are split into the incident (red), the compressed (blue) and the Raman-backscattered (RBS, orange, ×10 magnified). **c**, The compressed pulse in time. **d**. Power spectra of the incident (red), RBS (orange, ×10 magnified) and the compressed (blue) pulses.

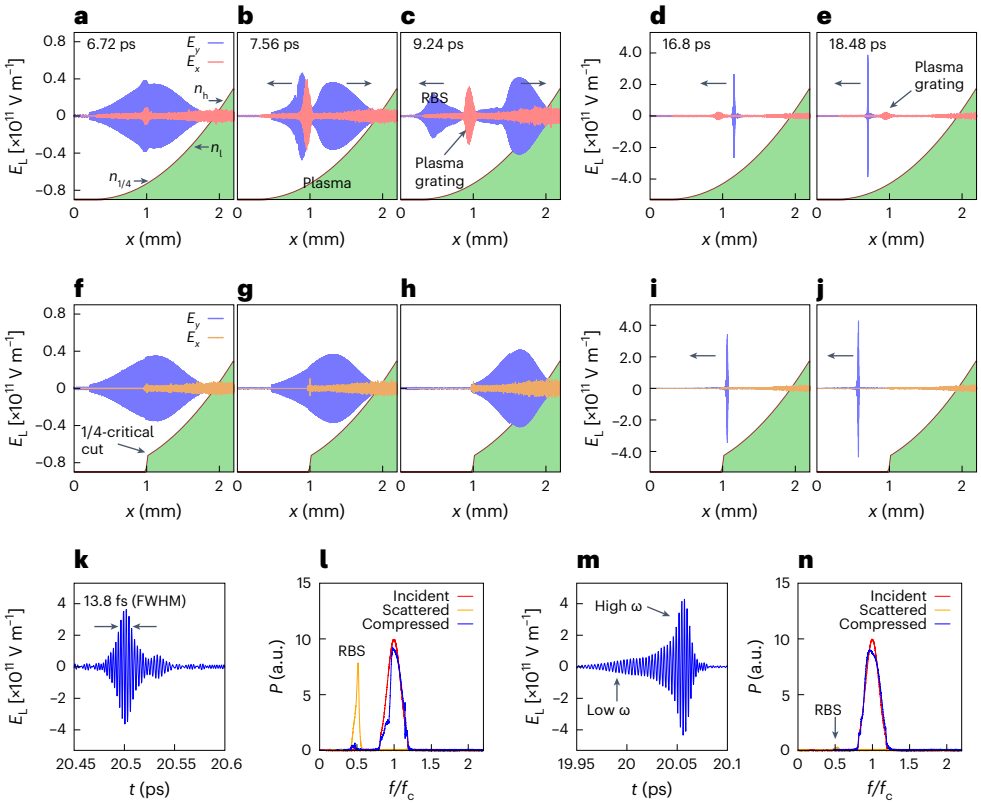

Fig. 3 | Effects of Raman backscatter on the pulse compression. **a**–**e**, Growth of RBS of the incident pulse in a thermal plasma ($T_e = 10$ eV) (**a**–**c**) and compressed pulse after reflection (**d**,**e**). **f**–**j**. Pulse compression under the same condition as **a**–**e** but with a quarter-cut plasma. **k**,**l**, Compressed pulse profile in time (**k**) and spectra of the incident (**l**), the compressed pulse and the RBS signal for a full parabolic density. The pulse duration represents the FWHM of intensity (square of the field). **m**,**n**. Pulse profile and spectra for the quarter-cut plasma.

spread out by thermal fluctuations. Figure 3l shows that the lower frequency component ($\omega/\omega_c < 1$, corresponding to the rear part of the pulse) is depleted, whereas a strong RBS peak appears at around half-critical frequency ($\omega/\omega_c \approx 0.5$). No signature of Raman forward scatter (RFS) is observed as the RFS growth rate is very small on the steep gradient. The compressed pulse passes through the plasma grating (the region of Raman-grown E_x) without backscattering (Fig. 3d,e).

As RBS occurs only for $n < n_{1/4}$, cutting out the plasma below the quarter-critical density can remedy energy loss by RBS. Note that the density cut naturally appears in free-expanding plasmas[28]. In Fig. 3f–h, E_x (orange) is considerably lower than in the full quadratic

https://doi.org/10.1038/s41566-023-01321-x

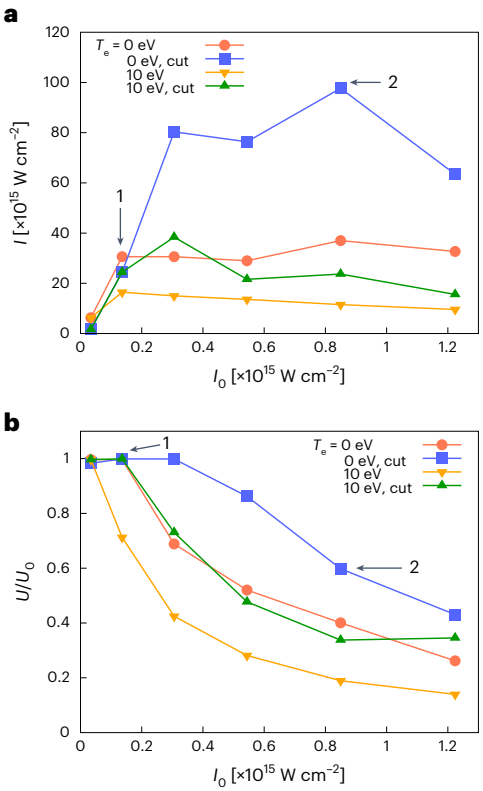

Fig. 4 | Characterization of pulse compression for varied laser intensity. **a**, Intensity of the compressed pulse versus the incident intensity for 0 and 10 eV, and full-quadratic and quarter-cut plasma. **b**, Ratio of the compressed pulse energy to the incident pulse energy. $U/U_0 = 1$ corresponds to no energy loss during compression.

case (Fig. 3a–c) and RBS is barely visible. As the part of the plasma is cut from the optimal quadratic density profile, the high-frequency components are slightly behind the low-frequency components (Fig. 3m). A higher gain could be obtained by increasing the density slope gradient. Total energy loss is much smaller (Fig. 3n) in the quarter-cut case.

In Fig. 4a we examine the intensity of the compressed pulse, varying the incident pulse intensity (I_0) and plasma temperature for full quadratic and quarter-cut plasma. For the full quadratic plasma, the compression saturates mostly for $I_0 > 10^{14}$ W cm^{-2}. With the quarter-cut plasmas, however, the saturation point is considerably delayed to $I_0 > 3 \times 10^{14}$ W cm^{-2}. Note that the points marked '1' and '2' in Fig. 4 correspond to the largest multiplication factor (225 times) and the maximum compressed intensity (~10^{17} W cm^{-2}), respectively, as described earlier.

Figure 4b shows the ratio of compressed pulse energy (U) to the incident pulse energy (U_0). In the incident range $2 \times 10^{14} < I_0 < 8 \times 10^{14}$ W cm^{-2}, the ratio for the quarter-cut plasma is up to twice that for the full quadratic plasma. Moreover, we would like to emphasize that RBS in PIC simulations is overestimated by numerically enhanced thermal noise. It is therefore possible that the saturation of compression or energy in Fig. 4 occurs at even higher intensities in real experiments, that is, it is improved.

Effects of fluctuation and instabilities

Density fluctuations and incidence angle

Local bumps or troughs in the plasma density profile can unfavourably affect the pulse compression as photons can be reflected earlier (by bumps) or later (by troughs) than in unperturbed density profiles. Change in the reflection time results in a spread of photons with respect to their fully compressed position. For a cosine-shaped bump or trough around the critical point, with amplitude δn_f and length $\lambda_f/2$, the relative change in reflection time of a photon is approximately

$$\frac{\Delta\tau_c}{\tau_\sigma} \simeq \frac{\delta n_f}{n_c}, \tag{1}$$

where τ_σ is the pulse duration (see Supplementary Fig. 4 for more details). This equation indicates that density fluctuations are detrimental to the efficiency of compression. Typically, the fluctuation level can be contained to roughly 1% in experiments, and one-hundred-fold pulse compression should be achievable, even with fluctuations. The radial fluctuation of density should be similarly small to suppress the deviation of photons in the transverse direction. For a higher compression rate, a specifically designed nonlinear chirp for faster compression, and highly tuned experimental techniques for suppressing the fluctuations, may be necessary.

Photon spread due to fluctuations in the low-density region (lower than the critical density) is insignificant compared with near-critical fluctuations, as alternating bumps and troughs tend to average out the travel-time deviation of photons. For $n \ll n_c$, the delay or advance of the photon's travel time is approximately $\delta n_f \lambda_f / (2cn_c)$. When there are $N \approx L/\langle\lambda_f\rangle$ bumps and troughs randomly distributed (N represents the number of bumps and troughs. L is the scale length of the density gradient), the accumulated change of the travel-time will occur as a random-walk, that is

$$\Delta\tau_l \approx \sqrt{N}\left\langle\frac{\delta n_f \lambda_f}{2cn_c}\right\rangle \approx \frac{\langle\delta n_f\rangle}{2n_c}\sqrt{\frac{\langle\lambda_f\rangle}{L}}\tau_\sigma. \tag{2}$$

For short wavelength fluctuations (that is, $\langle\lambda_f\rangle/L \ll 1$), $\Delta\tau_l \ll \Delta\tau_c$.

Variation of the incident angle, θ, either due to pointing jitter or focusing geometry, can reduce the reflection time by a factor of $\cos\theta$, resulting in a photon spread $\Delta\tau_c/\tau_\sigma \approx \theta^2/2$. To achieve hundred times compression, the angle should be smaller than ~100 mrad (~5.7°). Resonant heating due to the oblique p-polarized component of the pulse gives a stricter condition on the incidence angle. To maintain the fractional absorption (f_a) below 1%, from $f_a \approx \phi^2(\zeta)/2$, where $\zeta = (\omega L/c)^{1/3}\theta$ and ϕ is an absorption function[28], the incidence angle should be <10 mrad. The restriction of the incidence angle may require vacuum focusing over more than 10 m, which should be achievable, considering that focal lengths of modern petawatt systems are several metres[29].

In the above, we have relied on group-velocity calculations, which do not consider the bandwidth; however, a more rigorous calculation using Maxwell's equations indicates that group-velocity calculations are valid as long as the pulse bandwidth is dominated by the chirp, as in our case.

Parametric instabilities

Raman backscatter (RBS)[12] is the fastest growing instability that can lead to loss of photons. Fortunately, frequency chirps are known to suppress the growth of RBS[12,14,19], because the bandwidth of RBS resonance is very narrow. From the resonant bandwidth ~$\pi\gamma$ (ref. 19), the resonant portion $\Delta\tau_R$ in the pulse duration τ_σ is approximately given by $\Delta\tau_R/\tau_\sigma \approx \pi\gamma/\Delta\omega$, where $\Delta\omega$ is the bandwidth of the chirped pulse. The RBS growth rate, $\gamma = a_0\sqrt{\omega\omega_p}/2$ ($a_0 = eE_L/mc\omega$, that is, the normalized vector potential amplitude of the incident laser field, where m is the electron mass), reaches a maximum at the quarter-critical density ($\omega_p = \omega/2$), leading to $\Delta\tau_R/\tau_\sigma \simeq \pi a_0\omega/(2\Delta\omega)$. When the resonant portion of the pulse is completely depleted by RBS, the photon loss is under 10%, with $\Delta\omega/\omega \approx 0.1$, and we need $a_0 < 0.01$. The energy loss via RBS is 16% (Fig. 3), which coincides well with the estimate; however, we note that such a limitation in a_0 can be removed in diverse ways, for example, energy loss can be con-

siderably reduced by cutting out the plasma below the quarter-critical density, as we have shown.

Parametric decay into two plasmons[30] has a fast growth rate but a narrow bandwidth, which are both comparable with those of RBS. A similar loss of photons (about 10%) is expected, but as $2\omega_p$ grows at the quarter-critical density, the quarter-cut plasma used to suppress RBS will also be useful for suppressing two plasmon decay.

Raman forward scattering (RFS) has a growth rate of an order of magnitude lower than RBS and, moreover, is strongly suppressed in non-uniform plasma, and is negligible in our simulations, up to incident intensity 10^{16} W cm^{-2}. For an incident intensity ~10^{17} W cm^{-2}, substantial (8.5%) density deformation is observed due to ponderomotive force of the compressed pulse. Brillouin scattering is a much slower process than Raman and is therefore negligible.

Transverse instabilities

A wide laser pulse in high-density plasma can be subject to self-focusing[31], filamentation[32] and Rayleigh–Taylor-like instabilities[33]. For the moderate amplitude ($a_0 \approx 0.01$) and the supposed wide spot ($r_s \approx 1$ cm), the power before compression is well above the critical power for relativistic self-focusing, $P_c = 17.4\lambda_p^2/\lambda^2$ GW (ref. 31); however, for these parameters, the focal length induced by relativistic self-focusing, $z_{focus} \approx \omega r_s/(\omega_p a_0) \approx 100$ cm, is orders of magnitude longer than the plasma slabs used for the pulse compressor. Relativistic self-focusing can therefore be neglected or compensated for by downstream optics. The threshold for transverse ponderomotive channelling of plasma, given by $\sim (r_s/\lambda)^2 P_c$, is orders-of-magnitudes higher than P_c. Ponderomotive multifilamentation is another deleterious instability; its growth rate is given by $\gamma \approx \omega_{pi} a_0$ (ref. 32) (where ω_{pi} is the ion plasma frequency) and the time for one e-folding of filamentation for $a_0 \approx 0.01$ is ~10 ps, or longer, for heavier atoms, which exceeds the pulse duration considered. Therefore, ponderomotive filamentation, at most, has a marginally effect on the compression process. As will be shown, collisional heating is not effective and so thermal filamentation[34] can be neglected. The Rayleigh–Taylor-like instability occurs when a plasma is pushed forward by a strong ponderomotive front of the pulse, which is not relevant to our case.

Collisions and inverse bremsstrahlung

In fully ionized plasma, electron–ion collisions and subsequent inverse bremsstrahlung can deplete the pulse energy. The number of collisions experienced by a photon travelling towards the reflection point is $N_{col} = \int_0^{\tau_r} \nu_{ei}(t)\,dt \simeq \nu_{ei}\tau_r$, where τ_r is the travel time to the reflection point and ν_{ei} is the electron-ion collision frequency. Spitzer resistivity[35] gives the collision rate $\nu_{ei} \simeq 5\times10^{-12} n T_e^{-1.5}$ eV. With $n = n_c$, the ratio of N_{col} to the number of oscillations during the same period is $N_{col}/N_{osc} \simeq 5\pi\times10^{-12} n_c/(\omega T_e^{1.5})$. With $a_0 \approx 0.01$ and $T_e \approx mc^2\left(\sqrt{1+a_0^2}-1\right) \approx 20$ eV, we have $N_{col}/N_{osc} \leq 0.1$, implying that the pulse can lose at most 10% of its energy via collisions and inverse Bremsstrahlung on the path towards the reflection point. On the return path, the pulse amplitude is already increased by compression, which greatly reduces the collision rate.

Nonlinear chirp for realistic density profile

In experiments, the plasma density profile is not readily controllable. A freely expanding plasma takes on an exponential density profile[33], rather than a quadratic one. For this realistic scenario, the pulse chirp should be made nonlinear to obtain maximum compression (see the Supplementary Fig. 5), which can be achieved using standard ultrafast pulse shaping techniques[36]. It is relatively easy to generate an arbitrary pulse chirp to match a non-quadratic density profile. A non-uniform radial density profile of the laser-ablated plasma can lead to transversely different compression. A method should be devised to account for that effect, for example, phase-front-matching to the density contours by focusing or defocusing the pulses using deformable mirrors.

Conclusion

We have proposed a new method for laser pulse compression using a plasma slab with a density gradient. By tailoring the plasma density, the reflection path of high frequency components can be made longer than the path of low frequency components in a frequency-chirped long laser pulse. This idea has been verified using 1D PIC simulations, showing that a picosecond laser pulse can be compressed to few femtoseconds duration with a very high efficiency, exceeding 99%. The result indicates that a small plasma volume, with only 10 cm diameter, is sufficient to handle extremely high powers of up to 7.5 EW. Theoretical estimates verify that compression by hundred times can be obtained consistently even with density fluctuations and Raman instability. For the given laser pulse and plasma parameters, the compression process is well outside the deleterious effects of various transverse instabilities such as self-focusing and filamentation, implying that the compressed beam can maintain high quality in the transverse phase. The proposed idea should pave a new path toward compact exawatt-and-above high-power lasers in the future. Here we have laid the foundations of a new method by simulations only, with realistic effects that cannot be simulated being addressed theoretically. Realistic models that can be applied to experiments should be developed through 3D simulations of pulse compression and plasma generation processes.

Online content

Any methods, additional references, Nature Portfolio reporting summaries, source data, extended data, supplementary information, acknowledgements, peer review information; details of author contributions and competing interests; and statements of data and code availability are available at https://doi.org/10.1038/s41566-023-01321-x.

References

1. Strickland, D. & Mourou, G. Compression of amplified chirped optical pulses. *Opt. Comm.* **56**, 219–221 (1985).
2. Tajima, T., Yan, X. Q. & Ebisuzaki, T. Wakefield acceleration. *Rev. Mod. Plasma Phys.* **4**, 7 (2020).
3. Schreiber, J., Bolton, P. R. & Parodi, K. Invited Review Article: 'hands-on' laser-driven ion acceleration: a primer for laser-driven source development and potential applications. *Rev. Sci. Instrum.* **87**, 071101 (2016).
4. Piazza, A., Di, Müller, C., Hatsagortsyan, K. Z. & Keitel, C. H. Extremely high-intensity laser interactions with fundamental quantum systems. *Rev. Mod. Phys.* **84**, 1177 (2012).
5. Lundstrom, E. et al. Using high-power lasers for detection of elastic photon–photon scattering. *Phys. Rev. Lett.* **96**, 083602 (2006).
6. Blackburn, T. G. Radiation reaction in electron-beam interactions with high-intensity lasers. *Rev. Mod. Plasma Phys.* **4**, 5 (2020).
7. Sarri, G. et al. Generation of neutral and high-density electron-positron pair plasmas in the laboratory. *Nat. Comm.* **6**, 6747 (2015).
8. Schwinger, J. On gauge invariance and vacuum polarization. *Phys. Rev.* **82**, 664 (1951).
9. Chen, P. & Mourou, G. Accelerating plasma mirrors to investigate the black hole information loss paradox. *Phys. Rev. Lett.* **118**, 045001 (2017).
10. Stuart, B. C. et al. Optical ablation by high-power short-pulse lasers. *J. Opt. Soc. Am. B* **13**, 459–468 (1996).
11. Gamaly, E. G. et al. Ablation of solids by femtosecond lasers: ablation mechanism and ablation thresholds for metals and dielectrics. *Phys. Plasmas* **9**, 949–957 (2002).
12. Malkin, V. M., Shvets, G. & Fisch, N. J. Detuned Raman amplification of short laser pulses in plasma. *Phys. Rev. Lett.* **84**, 1208 (2000).

13. Shvets, G., Fisch, N. J., Pukhov, A. & Meyer-ter-Vehn, J. Superradiant amplification of an ultrashort laser pulse in a plasma by a counterpropagating pump. *Phys. Rev. Lett.* **81**, 4879 (1998).
14. Ersfeld, B. & Jaroszynski, D. A. Superradiant linear Raman amplification in plasma using a chirped pump pulse. *Phys. Rev. Lett.* **95**, 165002 (2005).
15. Cheng, W. et al. Reaching the nonlinear regime of Raman amplification of ultrashort laser pulses. *Phys. Rev. Lett.* **94**, 045003 (2005).
16. Ren, J., Cheng, W., Li, S. & Suckewer, S. A new method for generating ultraintense and ultrashort laser pulses. *Nat. Phys.* **3**, 732–736 (2007).
17. Trines, R. M. G. M. et al. Simulations of efficient Raman amplification into the multipetawatt regime. *Nat. Phys.* **7**, 87–92 (2011).
18. Hur, M. S. et al. Electron kinetic effects on Raman backscatter in plasmas. *Phys. Rev. Lett.* **95**, 115003 (2005).
19. Vieux, G. et al. Chirped pulse Raman amplification in plasma. *New J. Phys.* **13**, 063042 (2011).
20. Lancia, L. et al. Signatures of the self-similar regime of strongly coupled stimulated brillouin scattering for efficient short laser pulse amplification. *Phys. Rev. Lett.* **116**, 075001 (2016).
21. Lehmann, G. & Spatschek, K. H. Transient plasma photonic crystals for high-power lasers. *Phys. Rev. Lett.* **116**, 225002 (2016).
22. Lehmann, G. & Spatschek, K. H. Laser-driven plasma photonic crystals for high-power lasers. *Phys. Plasmas* **24**, 056701 (2017).
23. Wu, H.-C., Sheng, Z.-M. & Zhang, J. Chirped pulse compression in nonuniform plasma Bragg gratings. *Appl. Phys. Lett.* **87**, 201502 (2005).
24. Wu, H.-C. et al. Manipulating ultrashort intense laser pulses by plasma Bragg gratings. *Phys. Plasmas* **12**, 113103 (2005).
25. Vieux, G. et al. The role of transient plasma photonic structures in plasma-based amplifiers. *Commun. Phys.* **6**, 9 (2023).
26. Pervak, V. et al. Chirped-pulse amplification of laser pulses with dispersive mirrors. *Opt. Exp.* **17**, 19204–19212 (2009).
27. Birdsall, C. K. & Langdon, A. B. *Plasma Physics via Computer Simulation* Ch. 16 (Adam Hilger, 1991).
28. Kruer, W. L. *The Physics of Laser Plasma Interactions* Ch. 10 (Addison-Wesley, 1988).
29. Kim, H. T. et al. Stable multi-GeV electron acceleration driven by waveform-controlled PW laser pulses. *Sci. Rep.* **7**, 10203 (2017).
30. Liu, C. S. & Rosenbluth, M. N. Parametric decay of electromagnetic waves into two plasmons and its consequences. *Phys. Fluids* **19**, 967–971 (1976).
31. Sprangle, P., Tang, C. M. & Esarey, E. Relativistic self-focusing of short-pulse radiation beams in plasmas. *IEEE Trans. Plasma Sci.* **15**, 145–153 (1987).
32. Langdon, A. B. & Lasinski, B. F. Filamentation and subsequent decay of laser light in plasmas. *Phys. Rev. Lett.* **34**, 934–937 (1975).
33. Zhou, Y. et al. Rayleigh–Taylor and Richtmyer–Meshkov instabilities: a journey through scales. *Physica D* **423**, 132838 (2021).
34. Sodha, M. S., Ghatak, A. K. & Tripathi, V. K. Self focusing of laser beams in plasmas and semiconductors. *Prog. Opt.* **13**, 169–265 (1976).
35. Spitzer, L. Jr. & Harm, R. Transport phenomena in a completely ionized gas. *Phys. Rev.* **89**, 977–981 (1953).
36. Weiner, A. M. Ultrafast optical pulse shaping: a tutorial review. *Opt. Commun.* **284**, 3669–3692 (2011).

Methods

We used an in-house PIC code called cplPIC for the simulations, in which standard algorithms such as Boris mover[37] for particle motion, charge-conserving scheme of Buneman–Villasenor[38] for current calculation and staggered field solver on Yee mesh[39] are employed. The code has been verified through many of our previous studies[40] of laser–plasma interactions.

Data availability

The data supporting this study's findings and used for producing figures are freely available for reproduction from OSF public repository, at https://doi.org/10.17605/OSF.IO/RTF8Z.

Code availability

The code can be distributed under a collaborative agreement with UNIST CPL group.

References

37. Boris, J. P. & Shanny, R. A. in *Proc. Conf. Numerical Simulation of Plasmas (4th) Held at the Naval Reserarch Laboratory, Washington, D.C on 2,3 November 1970* 3–67 (Defense Technical Information Center, 1970).
38. Villasenor, J. & Buneman, O. Rigorous charge conservation for local electromagnetic field solvers. *Comp. Phys. Commun.* **69**, 306–316 (1992).
39. Yee, K. S. Numerical solution of initial boundary value problems involving Maxwell's equations in isotropic media. *IEEE Trans. Antennas Propag.* **14**, 302–307 (1966).
40. Kwon, K. B. et al. High-energy, short-duration bursts of coherent terahertz radiation from an embedded plasma dipole. *Sci. Rep.* **8**, 145 (2018).

Acknowledgements

This work was supported by the Basic Science Research Program through the National Research Foundation (NRF) of Korea (grant nos. NRF-2016R1A5A1013277, NRF-2020R1A2C1102236, NRF-2022R1A2C3013359, NRF-2022R1I1A1A01055853 and RS-2022-00154676). M.S.H. acknowledges support from HRD program for industrial innovation funded by KIAT of Korea Government MOTIE (grant no. P0023703). D.A.J., S.Y. and B.E. acknowledge support from the UK EPSRC (grant no. EP/N028694/1) and received funding from the European Union's Horizon 2020 research and innovation programme under grant agreement no. 871124, Laserlab-Europe. S.Y. and B.E. acknowledge support from the STFC (grant no. ST/G008248/1).

Author contributions

M.S.H., B.E., D.A.J. and H.S. conceived and developed the main idea and wrote the manuscript. M.S.H. conducted theoretical calculations and simulations. B.E. and S.Y. contributed to theoretical calculations. H.K., H.L., Y.L., M.K., H.S.S. and K.R. provided supplementary simulations. All authors commented on the manuscript.

Competing interests

The authors declare no competing interests.

Additional information

Supplementary information The online version contains supplementary material available at https://doi.org/10.1038/s41566-023-01321-x.

Correspondence and requests for materials should be addressed to Min Sup Hur, Dino A. Jaroszynski or Hyyong Suk.

Peer review information *Nature Photonics* thanks Kenan Qu and the other, anonymous, reviewer(s) for their contribution to the peer review of this work.